



Since January 2020 Elsevier has created a COVID-19 resource centre with free information in English and Mandarin on the novel coronavirus COVID-19. The COVID-19 resource centre is hosted on Elsevier Connect, the company's public news and information website.

Elsevier hereby grants permission to make all its COVID-19-related research that is available on the COVID-19 resource centre - including this research content - immediately available in PubMed Central and other publicly funded repositories, such as the WHO COVID database with rights for unrestricted research re-use and analyses in any form or by any means with acknowledgement of the original source. These permissions are granted for free by Elsevier for as long as the COVID-19 resource centre remains active.



## The inhibitory effects of PGG and EGCG against the SARS-CoV-2 3C-like protease



Wei-Chung Chiou<sup>a,1</sup>, Jui-Chieh Chen<sup>b,1</sup>, Yun-Ti Chen<sup>c</sup>, Jinn-Moon Yang<sup>c, d, e, f, g</sup>, Lih-Hwa Hwang<sup>h</sup>, Yi-Shuan Lyu<sup>a</sup>, Hsin-Yi Yang<sup>a</sup>, Cheng Huang<sup>a,\*</sup>

<sup>a</sup> Department of Biotechnology and Laboratory Science in Medicine, National Yang-Ming University, Taipei, Taiwan

<sup>b</sup> Department of Biochemical Science and Technology, National Chiayi University, Chiayi, Taiwan

<sup>c</sup> Institute of Bioinformatics and Systems Biology, National Chiao Tung University, Hsinchu, Taiwan

<sup>d</sup> Department of Biological Science and Technology, College of Biological Science and Technology, National Chiao Tung University, Hsinchu, Taiwan

<sup>e</sup> Center for Intelligent Drug Systems and Smart Bio-devices, National Chiao Tung University, Hsinchu, Taiwan

<sup>f</sup> Faculty of Internal Medicine, College of Medicine, Kaohsiung Medical University, Kaohsiung City, Taiwan

<sup>g</sup> Hepatobiliary Division, Department of Internal Medicine, Kaohsiung Medical University Hospital, Kaohsiung Medical University, Kaohsiung City, Taiwan

<sup>h</sup> Institute of Microbiology and Immunology, National Yang-Ming University, Taipei, Taiwan

### ARTICLE INFO

#### Article history:

Received 24 December 2020

Accepted 29 December 2020

Available online 6 January 2021

#### Keywords:

3CL protease (3CLpro)

COVID-19

EGCG

PGG

SARS-CoV-2

### ABSTRACT

The coronavirus disease (COVID-19) pandemic, resulting from human-to-human transmission of a novel severe acute respiratory syndrome coronavirus (SARS-CoV-2), has led to a global health crisis. Given that the 3 chymotrypsin-like protease (3CLpro) of SARS-CoV-2 plays an indispensable role in viral polyprotein processing, its successful inhibition halts viral replication and thus constrains virus spread. Therefore, developing an effective SARS-CoV-2 3CLpro inhibitor to treat COVID-19 is imperative. A fluorescence resonance energy transfer (FRET)-based method was used to assess the proteolytic activity of SARS-CoV-2 3CLpro using intramolecularly quenched fluorogenic peptide substrates corresponding to the cleavage sequence of SARS-CoV-2 3CLpro. Molecular modeling with GEMDOCK was used to simulate the molecular interactions between drugs and the binding pocket of SARS-CoV-2 3CLpro. This study revealed that the  $V_{max}$  of SARS-CoV-2 3CLpro was about 2-fold higher than that of SARS-CoV 3CLpro. Interestingly, the proteolytic activity of SARS-CoV-2 3CLpro is slightly more efficient than that of SARS-CoV 3CLpro. Meanwhile, natural compounds PGG and EGCG showed remarkable inhibitory activity against SARS-CoV-2 3CLpro than against SARS-CoV 3CLpro. In molecular docking, PGG and EGCG strongly interacted with the substrate binding pocket of SARS-CoV-2 3CLpro, forming hydrogen bonds with multiple residues, including the catalytic residues C145 and H41. The activities of PGG and EGCG against SARS-CoV-2 3CLpro demonstrate their inhibition of viral protease activity and highlight their therapeutic potentials for treating SARS-CoV-2 infection.

© 2021 Elsevier Inc. All rights reserved.

### 1. Introduction

SARS-CoV-2, a novel severe acute respiratory syndrome (SARS) coronavirus (CoV) that threatens the health and welfare of humans, has spread rapidly throughout the world's population since its first identification [1]. Among COVID-19 patients, the typical symptoms

include pneumonia, fever, breathing difficulty and lung infection, while many atypical symptoms have also been described [2]. With the current statistics of laboratory-confirmed cases and the deaths, elderly individuals with chronic cardiovascular diseases, diabetes or asthma are highly likely to experience severe or critical conditions upon SARS-CoV-2 infection, in a societal demographic [3]. Currently, there are no effective pharmacological drugs or vaccines against the virus [4].

The genome of enveloped  $\beta$  coronaviruses, including SARS-CoV-2, SARS-CoV and Middle East respiratory syndrome coronavirus (MERS-CoV), is delivered in the form of a positive-sense, single-stranded RNA, of about 26–32 kb in size, which encodes structural

\* Corresponding author. Department of Biotechnology and Laboratory Science in Medicine, National Yang-Ming University, Taipei, 11221, Taiwan.

E-mail addresses: [chengh@ym.edu.tw](mailto:chengh@ym.edu.tw) (C. Huang), [chengh521@gmail.com](mailto:chengh521@gmail.com) (C. Huang).

<sup>1</sup> These authors contributed equally to this work.

proteins (e.g., spike, envelope, membrane and nucleocapsid), nonstructural proteins (e.g., 3 chymotrypsin-like protease (3CLpro), papain-like protease (PLpro), helicase, RNA-dependent RNA polymerase (RdRp)), and accessory proteins [5]. In particular, 3CLpro catalyzes most of the proteolysis of polyprotein 1a and 1 ab, after self-cleavage from polyprotein 1a. With an amino acid sequence identity of 96% to SARS-CoV 3CLpro, differences in SARS-CoV-2 3CLpro are known to be T35V, A46S, S75 N, L86V, R88K, S94A, H134F, K180 N, L202V, A267S, T285A and I286L [6]. Given the role of 3CLpro in the life cycle of  $\beta$  coronaviruses, inhibition of viral 3CLpro effectually prevents viral replication in the host cell [7].

The use of natural compounds to treat infectious diseases has attracted the attention of the public, owing to their bioactivities and minimal side effects [8]. As a matter of fact, many natural compounds have shown broad-spectrum anti-coronavirus activities, particularly against SARS-CoV 3CLpro [9]. Although the virtual identification of potential SARS-CoV-2 3CLpro inhibitors has been performed in a phytochemical library [10], the therapeutic potentials of candidates for COVID-19 treatment require further evaluation. 1,2,3,4,6-pentagalloylglucose (PGG), a hydrolysable, anti-inflammatory tannin, has been reported to inhibit herpes simplex virus type 1 (HSV-1), influenza A virus (IAV), human respiratory syncytial virus (hRSV) and human rhinoviruses (hRVs) [11]. The antiviral activity of PGG is known to involve direct inactivation, inhibition of virus adsorption to host cells, and inhibition of viral gene expression and protein translation [11]. As the most abundant catechin in green tea, (–)-epigallocatechin-3-gallate (EGCG) is the ester of epigallocatechin and gallic acid. EGCG has been described as a powerful antioxidant and anti-inflammatory, antibacterial, and antiviral agent that can modulate lipid metabolism and other metabolic pathways [12]. In particular, Zuo et al. demonstrated the inhibitory activity of EGCG on hepatitis C virus (HCV) NS3 serine protease [13].

Aiming to provide a therapeutic strategy against SARS-CoV-2 infectin, we first investigated whether amino acid differences in SARS-CoV-2 3CLpro influence the proteolytic efficiency, compared to SARS-CoV 3CLpro using fluorescence resonance energy transfer (FRET) based internally quenched fluorescent (IQF) peptide substrates. Then, we determined the potential of phytochemicals for SARS-CoV-2 3CLpro inhibition. Subject to the extent of SARS-CoV-2 3CLpro inhibition, the half maximal inhibitory concentrations of compounds of interest were determined subsequently. In parallel, compounds of interest were analyzed by computational molecular docking, thereby unraveling their mechanisms of action (MOA).

## 2. Materials and methods

### 2.1. Plasmids pET28b-SARS-CoV-2-3CLpro and pET28b-3CLpro

The DNA sequence encoding 3CLpro [14] was chemically synthesized by Mission Biotech, Taiwan. The full sequence of 3CLpro was amplified with ExcelTaq™ Taq DNA polymerase (Smobio, Taiwan) using primers 5'-ATGGGTCGGGATCCCAGTGGTTTAAAGAA-3' and 5'-GGTGCTCGAGTTCATCTAGTTATTGGAAAGTAACACTGAG-3', and subcloned into a T7-based pET-28b(+) plasmid (Thermo Fisher Scientific, USA) with BamHI and XhoI restriction sites. The construct was verified by DNA sequencing. The plasmid pET28b-3CLpro which contains the SARS-CoV 3CLpro cDNA sequence was constructed as reported previously [15].

### 2.2. Protein expression, purification, and western blot analysis

The 3CLpro proteins were expressed in *E. coli* and purified as described previously [15]. The purified protein quality was more than 95%. The western blot analysis followed the protocol described

previously [16].

### 2.3. Protease activity assays and enzyme kinetics using IQF peptide substrates

The establishment of an Edans-Dabcyl (ED) FRET platform followed the published protocol [17]. Briefly, an internally quenched fluorescent (IQF) peptide containing a consensus cleavage sequence recognized by the 3CLpro of SARS-CoV and SARS-CoV-2 was synthesized by Genomics, Taiwan, with DABCYL at the N-terminal and EDANS at the C-terminal end, respectively—DABCYL-TSAVLQ↓SGFRKME-EDANS. Protease activity assays were performed using 0.125  $\mu$ M enzyme and 1.25  $\mu$ M peptide substrate. The kinetic parameters were determined using 0.125  $\mu$ M enzyme and 0–100  $\mu$ M peptide substrate, followed by the analysis published previously [14]. Measurements of the spectral-based fluorescence were determined by a SPARK® multimode microplate reader (TECAN, Switzerland) with the excitation at 355 nm at a bandwidth of 10 nm and the emission at 538 nm at a bandwidth of 15 nm. The relative fluorescence unit (RFU) was obtained at a gain of 131 in Spark® Control Magellan™ v2.2 software.

### 2.4. Chemicals

Natural compounds used in this study were purchased from Sigma-Aldrich, USA, dissolved in DMSO at a final concentration of 100 mM, and stored at  $-20^{\circ}\text{C}$  before use.

### 2.5. Dose-response curve analysis

Prior to the addition of IQF peptide substrates, 0.125  $\mu$ M SARS-CoV-2 3CLpro was incubated with the compound at the indicated concentration for one hour at  $37^{\circ}\text{C}$ . Later, IQF peptide was added at a final concentration of 1.25  $\mu$ M and incubated for three hours at  $37^{\circ}\text{C}$ . Fluorescence detection follows the procedure in protease activity assays. Points of relative protease activity upon the treatment of a compound at a concentration of 0–100  $\mu$ M were fitted to a normalized dose-response (variable slope) model in GraphPad Prism 7.03 for  $\text{IC}_{50}$  characterization.

### 2.6. Molecular modeling

The molecular simulation docking of PGG and EGCG into the binding site of SARS-CoV-2 3CLpro was explored using software GEMDOCK [18]. The 3D structures of PGG and EGCG were obtained from DrugBank [19]. The structure of SARS-CoV-2 3CLpro was extracted from the co-crystal structure [14] on Protein Data Bank (PDB). The interacting residues in the binding pocket of SARS-CoV-2 3CLpro were defined by an 8 Å-radius sphere around the bound peptide-like inhibitor PRD\_002214, and the coordinates of the atoms in the binding pocket were retrieved from the PDB.

### 2.7. Statistical analysis

Data collected in the study were analyzed and plotted with GraphPad Prism 7.03. Values were expressed as the mean  $\pm$  standard error mean (SEM). For determination of the statistical significance between two groups, Student's t-tests were performed. For multiple comparisons between the treated conditions to the control, one-way ANOVA post hoc Dunnett's multiple comparisons tests were performed. Statistical significance was expressed as  $P < 0.05$  (e.g., \*),  $p < 0.01$  (e.g., \*\*), and  $p < 0.001$  (e.g., \*\*\*).

### 3. Results

#### 3.1. The proteolytic efficiency of SARS-CoV-2 3CLpro

Recombinant SARS-CoV 3CLpro and SARS-CoV-2 3CLpro were expressed in *E. coli* and purified by single-step affinity chromatography using the N-terminal His-tag. As shown in Fig. 1A, the expressed proteins were of high homogeneity, with a size of about 37.4 kDa, corresponding to the predicted size and correlating with our previous finding [15]. Using IQF peptide substrates, the proteolytic efficiency of SARS-CoV-2 3CLpro was investigated in parallel with SARS-CoV 3CLpro. To determine the proteolytic efficiency, the detected RFUs were converted to Edans concentrations, using the linear regression in Fig. 1B. The velocity of SARS-CoV-2 3CLpro was significantly higher than SARS-CoV 3CLpro (Fig. 1C). In Fig. 1D, the kinetic parameters are plotted side by side. Specifically, the  $K_m$  value of the IQF peptide substrate for SARS-CoV-2 3CLpro was 78.69  $\mu\text{M}$ , the  $V_{\max}$  was 20.18  $\mu\text{M}/\text{min}$ , the  $K_{\text{cat}}$  was 322.88  $\text{min}^{-1}$ , and the  $K_{\text{cat}}/K_m$  was 68386.50  $\text{M}^{-1} \text{s}^{-1}$ ; in comparison, the  $K_m$ ,  $V_{\max}$ ,  $K_{\text{cat}}$ , and  $K_{\text{cat}}/K_m$  of SARS-CoV 3CLpro were 42.34  $\mu\text{M}$ , 10.81  $\mu\text{M}/\text{min}$ , 172.96  $\text{min}^{-1}$ , and 68083.77  $\text{M}^{-1} \text{s}^{-1}$ , respectively. An approximately 2-fold higher  $V_{\max}$  was seen for SARS-CoV-2 3CLpro, compared to SARS-CoV 3CLpro, while the  $K_m$  of SARS-CoV-2 3CLpro was slightly higher than that of SARS-CoV 3CLpro, indicating that the difference in proteolytic efficiency is more pronounced at a high substrate concentration. Moreover, the cumulative yield curve of SARS-CoV-2 3CLpro at 37 °C over time is depicted and SARS-CoV-2 3CLpro was shown to have a greater proteolytic efficiency, compared to SARS-CoV 3CLpro (Fig. 1E).

When the protease and substrate concentrations were at a similar level, SARS-CoV 3CLpro and SARS-CoV-2 3CLpro reached the peak of their yield three hours after the addition of the substrate at 37 °C. In particular, the activity of SARS-CoV-2 3CLpro was 1.3-fold higher than that of SARS-CoV 3CLpro at the 3-hr time point, as shown in Fig. 1F. Taken together, the results show that the proteolytic activity of SARS-CoV-2 3CLpro is more efficient than SARS-CoV 3CLpro.

#### 3.2. Screening of compounds against SARS-CoV-2 3CLpro activity

To evaluate the inhibitory activity of compounds against SARS-CoV-2 3CLpro, a screening platform was established using FRET-based IQF peptide substrates to characterize the relative enzymatic activity, with or without compound treatment. Over 60 natural compounds were screened for SARS-CoV-2 3CLpro inhibitory activity at 20  $\mu\text{M}$ . The inhibitory effect of twelve well-known phytochemicals on 3CLpro activity at 20  $\mu\text{M}$  is shown in Fig. 2. It is worthwhile to mention that coumaric acid, rotenone, catechin, (–)-epicatechin gallate (ECG), ursolic acid and fenofibrate had a greater inhibitory activity against SARS-CoV 3CLpro than against SARS-CoV-2 3CLpro. Interestingly, PGG and EGCG had a selectivity for the inhibition of SARS-CoV-2 3CLpro over the SARS-CoV enzyme. Specifically, PGG and EGCG inhibited SARS-CoV-2 3CLpro activity by 85% and 91% respectively, and SARS-CoV 3CLpro by 73% and 49% respectively. Taken together, PGG and EGCG exhibited distinct inhibitory activity against SARS-CoV-2 3CLpro.

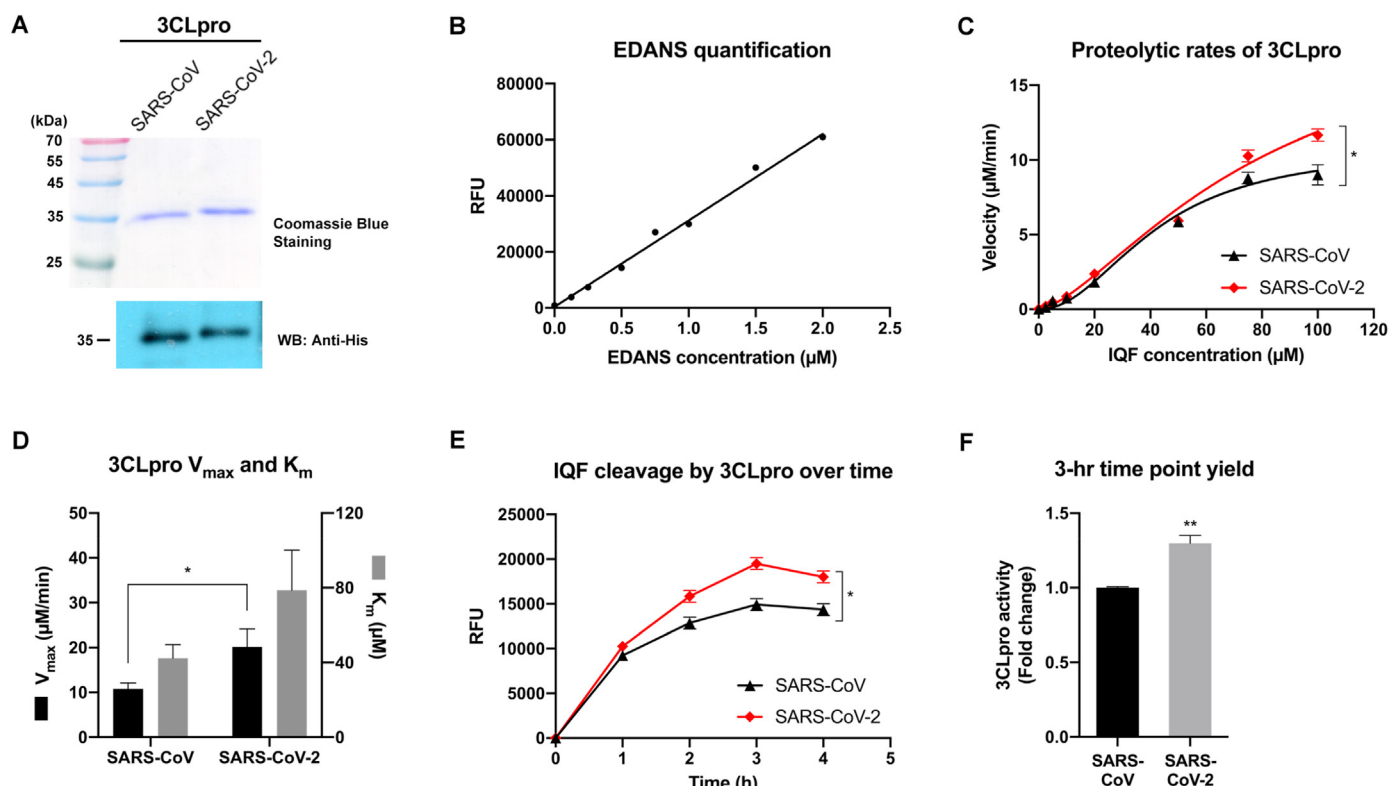


**Fig. 1. The proteolytic activity of recombinant SARS-CoV-2 3CLpro.** (A) Coomassie blue staining and western blot analysis of His-tagged 3CLpro. (B) Edans quantification. The RFU was plotted with respect to each free Edans concentration. (C) 3CLpro catalyzed substrate proteolytic rate at different IQF peptide substrate concentrations. The velocities of SARS-CoV 3CLpro and SARS-CoV-2 3CLpro were determined. (D) Kinetic parameters of SARS-CoV 3CLpro and SARS-CoV-2 3CLpro. From the fitted curve shown in (B), the  $V_{\max}$  (black) and  $K_m$  (gray) of SARS-CoV-2 3CLpro were characterized, with SARS-CoV 3CLpro shown alongside. (E) Cleavage of IQF peptide substrates by 3CLpro over time. (F) Yield of IQF substrate cleavage by 3CLpro at the 3-hr time point. Data (N = 3) are expressed as the mean  $\pm$  SEM (\*:  $p < 0.05$ , \*\*:  $p < 0.01$ , \*\*\*:  $p < 0.001$ ). (For interpretation of the references to color in this figure legend, the reader is referred to the Web version of this article.)

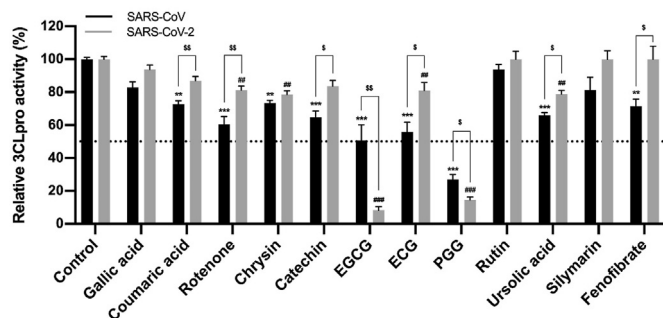


**Fig. 2. Screening for candidates of 3CLpro inhibitors.** The inhibitory activities of natural compounds against SARS-CoV-2 3CLpro were compared in parallel with SARS-CoV 3CLpro. Changes in the 3CLpro activity were normalized by the corresponding control. The dotted line indicates 50% of 3CLpro activity. Drugs vs. control in the SARS-CoV group: \*,  $p < 0.05$ ; \*\*,  $p < 0.01$ ; \*\*\*,  $p < 0.001$ ; Drugs vs. control in the SARS-CoV-2 group: #,  $p < 0.05$ ; ##,  $p < 0.01$ ; ###,  $p < 0.001$ , using one-way ANOVA post hoc Dunnett's multiple comparisons tests. Each drug in SARS-CoV vs. in SARS-CoV-2: \$,  $p < 0.05$ ; \$\$,  $p < 0.01$ , using Student's *t*-tests.

### 3.3. The inhibitory effects of PGG and EGCG on SARS-CoV-2 and SARS-CoV 3CLpro

To determine the  $IC_{50}$  values of PGG and EGCG against SARS-CoV-2 3CLpro, these agents were added to the protease activity

assay at various concentrations. PGG inhibited 50% of SARS-CoV-2 3CLpro and SARS-CoV 3CLpro at  $3.66 \pm 0.02 \mu\text{M}$  and  $6.89 \pm 0.15 \mu\text{M}$ , respectively (Fig. 3A and B); while EGCG had an  $IC_{50}$  value of  $4.24 \pm 0.16 \mu\text{M}$  with respect to SARS-CoV-2 3CLpro, as opposed to  $24.98 \pm 4.03 \mu\text{M}$  with respect to SARS-CoV 3CLpro (Fig. 3C and D). Specifically, PGG had the best inhibitory activity against SARS-CoV-2 3CLpro, followed by EGCG, highlighting their therapeutic potentials for treating SARS-CoV-2 infection.

### 3.4. Molecular modeling of PGG or EGCG in the binding pocket of SARS-CoV-2 3CLpro

It has been shown that the substrate binding pocket of SARS-CoV-2 3CLpro can be divided into four subsites, where subsite 1 (S1) contains F140, L141, M165, E166 and H163, subsite 1' (S1') includes N142, G143, S144 and C145, subsite 2 (S2) comprises H41, M49, R188 and Q189, and subsite 4 (S4) comprises T190, A191, and P168 [14]. In order to study the binding mechanisms of PGG and EGCG, we integrated molecular docking GEMDOCK to predict the docked conformations in the active site of 3CLpro, based on the calculated binding energies. The subsites (S1, S1', S2 and S4) of the substrate binding pocket and catalytic residues of SARS-CoV-2 3CLpro are illustrated in Fig. 4A. In the binding model of PGG, PGG occupies the S1, S1' and S4 subsites of SARS-CoV-2 3CLpro, forming hydrogen bonds with multiple residues, including the catalytic residue C145 ( $-6.4 \text{ kcal/mol}$ ) (Fig. 4B and D). PGG extends

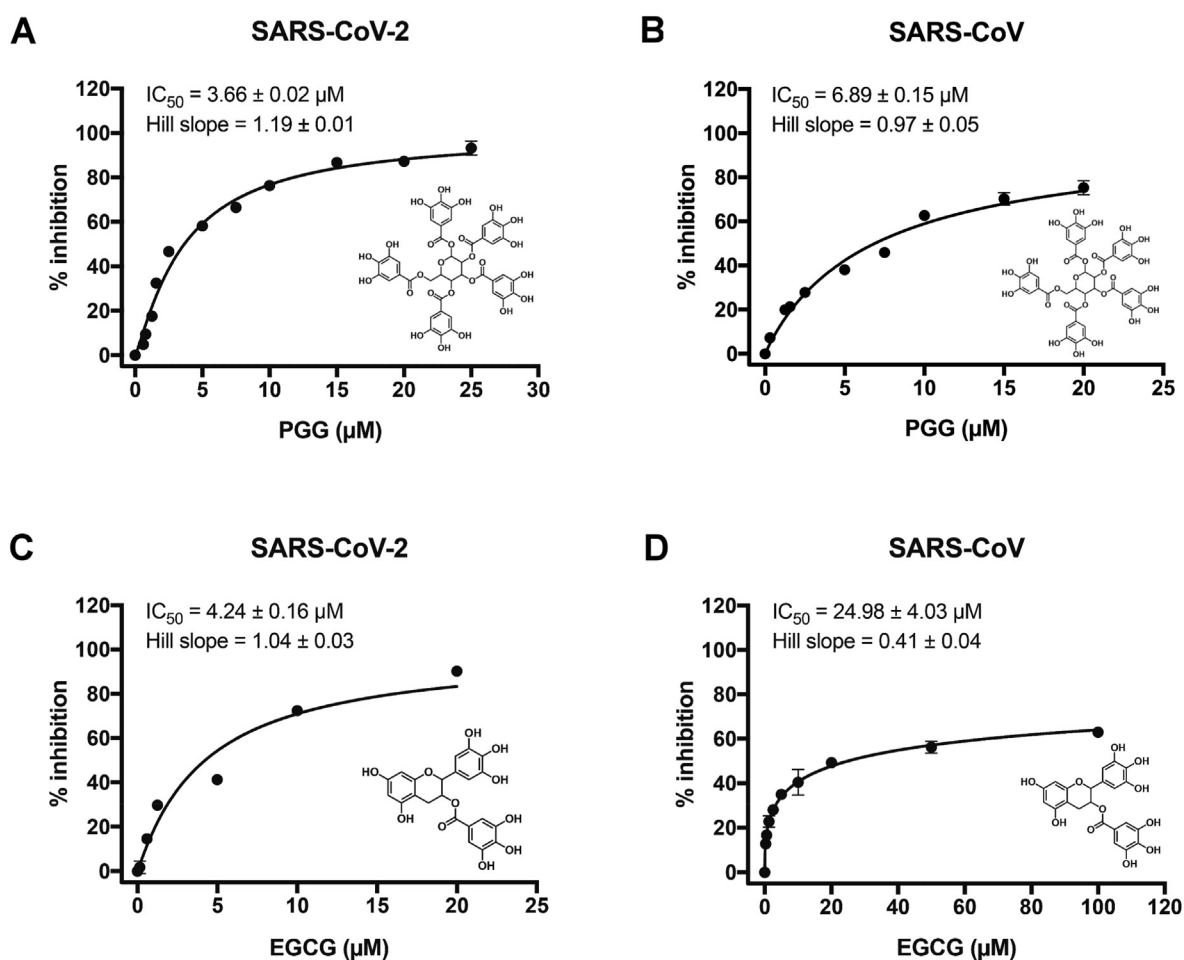


**Fig. 3. Inhibitory effects of PGG and EGCG on SARS-CoV-2 3CLpro.** (A–D) Dose-response curves of PGG and EGCG against SARS-CoV-2 3CLpro and SARS-CoV 3CLpro. Changes in the relative SARS-CoV 3CLpro activity (B and D) and the relative SARS-CoV-2 3CLpro activity (C and E) are shown. Data ( $N = 3$ ) are expressed as the mean  $\pm$  SEM.

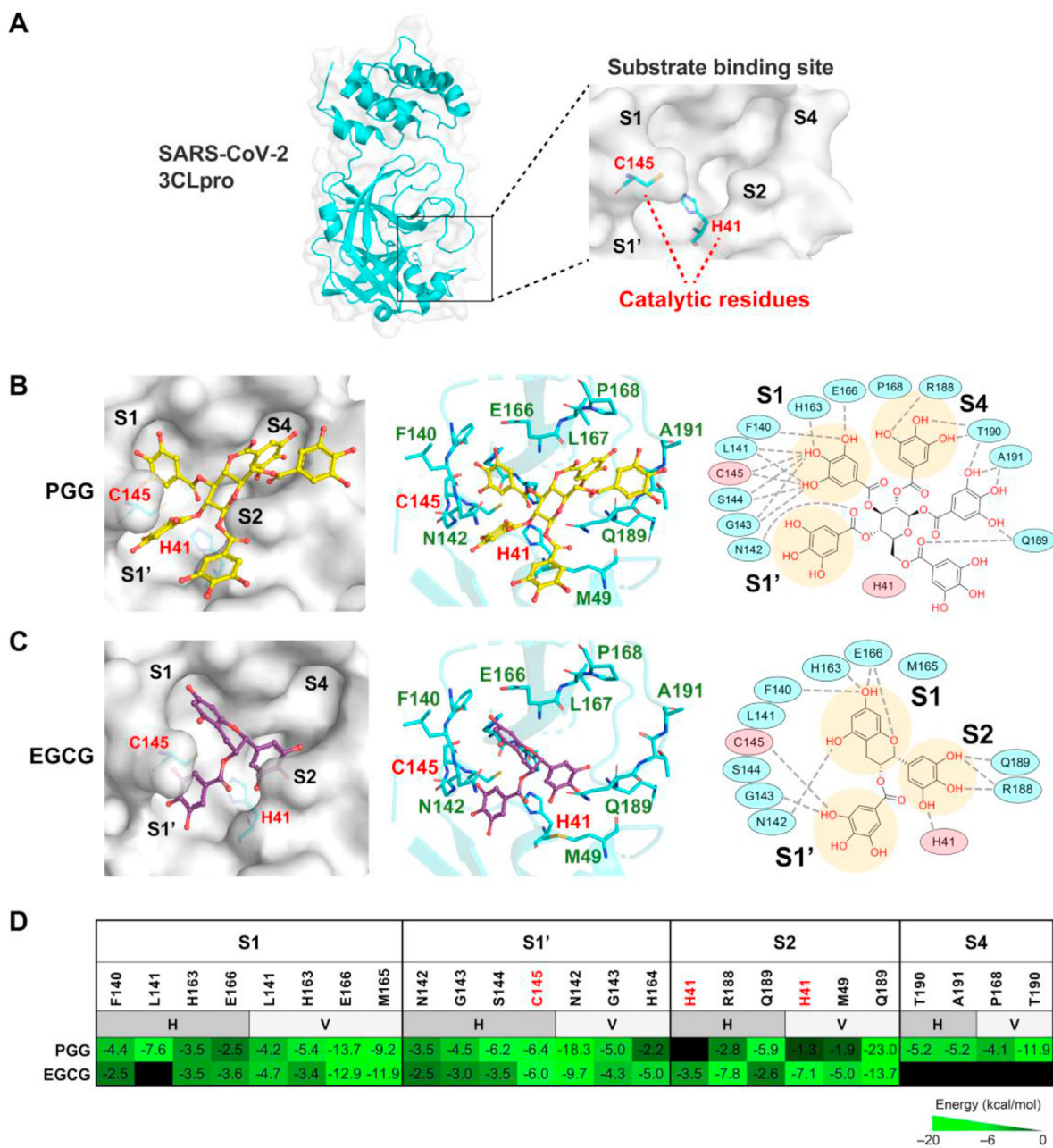


**Fig. 4. Molecular modeling of PGG and EGCG in the binding pocket of SARS-CoV-2 3CLpro.** (A) Ribbon diagram of SARS-CoV-2 3CLpro with a vacant substrate binding site. S1, S1', S2 and S4 subsites are labeled (black), along with the catalytic residues (red), H41 and C145. (B–C) PGG (B) and EGCG (C) docking in SARS-CoV-2 3CLpro. Left: PGG (yellow) and EGCG (purple) are depicted with balls and sticks, while the 3D binding pocket is shown in shaded white. The locations of the catalytic residues and subsites are labeled in red and black, respectively. Middle: The main residues (cyan) of SARS-CoV-2 3CLpro around PGG (yellow) or EGCG (purple) in the binding pocket are labeled, including the catalytic residues. Right: Amino acids engaged in the binding of PGG or EGCG are arrayed around the chemical structure, with the involved subsites shaded in beige. Hydrogen bonds are shown as gray dashed lines, while the Van der Waals forces have been omitted from the diagram for simplicity. (D) Interaction energy (kcal/mol) between PGG or EGCG and the residues of SARS-CoV-2 3CLpro. The crucial interacting residues of SARS-CoV-2 3CLpro in the binding models of PGG and EGCG are shown at the top, with catalytic residues highlighted in red. The involved types of forces, hydrogen (H) and/or Van der Waals (V), were indicated above each interaction energy. The strength of the interaction is correlated positively with the brightness of the color; no interaction is shown in black. (For interpretation of the references to color in this figure legend, the reader is referred to the Web version of this article.)

to the S4 subsite, with its five gallic acids, and forms hydrogen bonds with T190 and A191. As for the binding of EGCG, EGCG occupies the S1, S1' and S2 subsites of SARS-CoV-2 3CLpro, forming hydrogen bonds at both catalytic residues (H41,  $-3.5$  kcal/mol and C145,  $-6.0$  kcal/mol) (Fig. 4C and D). All hydrogen and Van der Waals forces involved in the binding of PGG or EGCG are listed in Fig. 4D. Regarding the number of subsite contacts and the binding

energy of each interaction, both PGG and EGCG showed efficient inhibition on SARS-CoV-2 3CLpro by strong interaction with the substrate binding pocket. Comparison of the binding model of PGG and EGCG in this pocket reveals that PGG may exhibit greater inhibition than EGCG because of the occupied pocket and the energy, corresponding to the *in vitro* results presented above.

#### 4. Discussion

The current coronavirus outbreak, attributable to SARS-CoV-2, has not only distressed the health and welfare of humans but also imposed burdens on worldwide economic activity and development. The efficiency of viral proteases in the cytosol can potentially influence the replication rate of the virus in the host [20]. Here, we found that the  $V_{\max}$  of SARS-CoV-2 3CLpro in the experimental conditions was about 2-fold greater than that of SARS-CoV 3CLpro. The replication rate is generally dictated by the proteolytic efficiency of 3CLpro, replication of the viral genome, and the assembly of viral particles [7]. Given that the processing of viral polyproteins of SARS-CoV-2 depends greatly on 3CLpro, the higher proteolytic efficiency of SARS-CoV-2 3CLpro could accelerate the viral life cycle. In support of our findings, recent studies have shown that the viral load in patients governs the transmission potential of SARS-CoV-2, regardless of the development of symptoms [21].

Here, we identified two 3CLpro inhibitors, PGG and EGCG, which have excellent inhibitory activity against SARS-CoV-2 3CLpro. Despite the structural similarity between EGCG and ECG, Zuo et al. demonstrated that the inhibitory effect of EGCG on HCV NS3-4A serine protease was more potent than that of ECG [13]. Interestingly, we also observed a more efficient inhibition of SARS-CoV-2 3CLpro by EGCG than ECG. Recently, the anti-SARS-CoV-2 3CLpro activity of EGCG and theaflavin had been reported, with  $IC_{50}$  values of 7.58 and 8.44  $\mu\text{g/mL}$ , respectively [22]. In support of the anti-SARS-CoV-2 3CLpro activity of PGG, a derivative of PGG, tetragalloylglucose, was proved to have the anti-SARS-CoV activity [23]. In particular, both PGG and EGCG formed hydrogen bonds and Van der Waals forces with multiple residues, including those involved in the catalytic activity, in the binding pocket of SARS-CoV-2 3CLpro. The binding profiles of PGG and EGCG in SARS-CoV-2 3CLpro inhibition correspond to the results of a recent study [14], where successful protease inhibition occludes the accessibility of the substrate binding site and the catalytic residues. Besides, PGG showed greater inhibition of SARS-CoV-2 3CLpro than EGCG. The docked conformations of PGG and EGCG differ, which may result in the different inhibition *in vitro*. However, the activities of PGG and EGCG against SARS-CoV-2 *in vivo* need further investigation.

The results of a recent study suggest that the high death rate of severe COVID-19 patients might be due partly to hyperinflammation, resulting from a virus-activated cytokine storm syndrome, or fulminant myocarditis [24]. Thus, urgent treatment with anti-inflammatory agents at the onset of cytokine storm syndrome is considered to be beneficial to prevent multiorgan failure [25]. As the anti-inflammatory activities of PGG and EGCG have been described and widely elucidated [26,27], the newly characterized functionality of PGG and EGCG to SARS-CoV-2 3CLpro inhibition demonstrated in this study indicates their potential therapeutic use in COVID-19 treatment as dual-functional molecules.

In conclusion, the 3CLpro inhibition by PGG and EGCG is to occlude peptide substrates from access to the catalytic residues C145 and H41 and therefore to suppress viral protein production and to repress viral replication. Both PGG and EGCG are of great promise in relieving the medical distress caused by SARS-CoV-2 and other viral infections involving proteolysis of viral polyproteins.

#### Declaration of competing interest

The authors declare no conflicts of interest in regards to this manuscript.

#### Acknowledgements

This work was supported by research grant MOST 109-2327-B-010-005 from the Ministry of Science and Technology, Taiwan.

#### References

- [1] W.J. Guan, Z.Y. Ni, Y. Hu, W.H. Liang, C.Q. Ou, J.X. He, L. Liu, H. Shan, C.L. Lei, D.S.C. Hui, B. Du, L.J. Li, G. Zeng, K.Y. Yuen, R.C. Chen, C.L. Tang, T. Wang, P.Y. Chen, J. Xiang, S.Y. Li, J.L. Wang, Z.J. Liang, Y.X. Peng, L. Wei, Y. Liu, Y.H. Hu, P. Peng, J.M. Wang, J.Y. Liu, Z. Chen, G. Li, Z.J. Zheng, S.Q. Qiu, J. Luo, C.H. Ye, S.Y. Zhu, N.S. Zhong, C. China Medical Treatment, Expert group for, clinical characteristics of coronavirus disease 2019 in China, *N. Engl. J. Med.* 382 (2020) 1708–1720, <https://doi.org/10.1056/NEJMoa2002032>.
- [2] S.P. Adhikari, S. Meng, Y.J. Wu, Y.P. Mao, R.X. Ye, Q.Z. Wang, C. Sun, S. Sylvia, S. Rozelle, H. Raat, H. Zhou, Epidemiology, causes, clinical manifestation and diagnosis, prevention and control of coronavirus disease (COVID-19) during the early outbreak period: a scoping review, *Infect Dis Poverty* 9 (2020) 29, <https://doi.org/10.1186/s40249-020-00646-x>.
- [3] F. Zhou, T. Yu, R. Du, G. Fan, Y. Liu, Z. Liu, J. Xiang, Y. Wang, B. Song, X. Gu, L. Guan, Y. Wei, H. Li, X. Wu, J. Xu, S. Tu, Y. Zhang, H. Chen, B. Cao, Clinical course and risk factors for mortality of adult inpatients with COVID-19 in Wuhan, China: a retrospective cohort study, *Lancet* 395 (2020) 1054–1062, [https://doi.org/10.1016/S0140-6736\(20\)30566-3](https://doi.org/10.1016/S0140-6736(20)30566-3).
- [4] R. Wu, L. Wang, H.D. Kuo, A. Shannar, R. Peter, P.J. Chou, S. Li, R. Hudlikar, X. Liu, Z. Liu, G.J. Poiani, L. Amorosa, L. Brunetti, A.N. Kong, An update on current therapeutic drugs treating COVID-19, *Curr Pharmacol Rep* (2020) 1–15, <https://doi.org/10.1007/s40495-020-00216-7>.
- [5] G. Li, E. De Clercq, Therapeutic options for the 2019 novel coronavirus (2019-nCoV), *Nat. Rev. Drug Discov.* 19 (2020) 149–150, <https://doi.org/10.1038/d41573-020-00016-0>.
- [6] X. Liu, X.J. Wang, Potential inhibitors against 2019-nCoV coronavirus M protease from clinically approved medicines, *J Genet Genomics* 47 (2020) 119–121, <https://doi.org/10.1016/j.jgg.2020.02.001>.
- [7] E. de Wit, N. van Doremalen, D. Falzarano, V.J. Munster, SARS and MERS: recent insights into emerging coronaviruses, *Nat. Rev. Microbiol.* 14 (2016) 523–534, <https://doi.org/10.1038/nrmicro.2016.81>.
- [8] M. Tahir Ul Qamar, A. Maryam, I. Muneer, F. Xing, U.A. Ashfaq, F.A. Khan, F. Anwar, M.H. Geesi, R.R. Khalid, S.A. Rauf, A.R. Siddiqi, Computational screening of medicinal plant phytochemicals to discover potent pan-serotype inhibitors against dengue virus, *Sci. Rep.* 9 (2019) 1433, <https://doi.org/10.1038/s41598-018-38450-1>.
- [9] M.T. Islam, C. Sarkar, D.M. El-Kersh, S. Jamaddar, S.J. Uddin, J.A. Shilpi, M.S. Mubarak, Natural products and their derivatives against coronavirus: a review of the non-clinical and pre-clinical data, *Phytother. Res.* (2020), <https://doi.org/10.1002/ptr.6700>.
- [10] C. Wu, Y. Liu, Y. Yang, P. Zhang, W. Zhong, Y. Wang, Q. Wang, Y. Xu, M. Li, X. Li, M. Zheng, L. Chen, H. Li, Analysis of therapeutic targets for SARS-CoV-2 and discovery of potential drugs by computational methods, *Acta Pharm. Sin. B* (2020), <https://doi.org/10.1016/j.apsb.2020.02.008>.
- [11] C. Torres-León, J. Ventura-Sobrevilla, L. Serna-Cock, J.A. Ascacio-Valdés, J. Contreras-Esquível, C.N. Aguilar, Pentagalloylglucose (PGG): a valuable phenolic compound with functional properties, *Journal of Functional Foods* 37 (2017) 176–189, <https://doi.org/10.1016/j.jff.2017.07.045>.
- [12] A. Granja, I. Frias, A.R. Neves, M. Pinheiro, S. Reis, Therapeutic potential of epigallocatechin gallate nanodelivery systems, *BioMed Res. Int.* 2017 (2017) 5813793, <https://doi.org/10.1155/2017/5813793>.
- [13] G. Zuo, Z. Li, L. Chen, X. Xu, Activity of compounds from Chinese herbal medicine Rhodiola kirilowii (Regei) Maxim against HCV NS3 serine protease, *Antiviral Res.* 76 (2007) 86–92, <https://doi.org/10.1016/j.antiviral.2007.06.001>.
- [14] Z. Jin, X. Du, Y. Xu, Y. Deng, M. Liu, Y. Zhao, B. Zhang, X. Li, L. Zhang, C. Peng, Y. Duan, J. Yu, L. Wang, K. Yang, F. Liu, R. Jiang, X. Yang, T. You, X. Liu, X. Yang, F. Bai, H. Liu, X. Liu, L.W. Guddat, W. Xu, G. Xiao, C. Qin, Z. Shi, H. Jiang, Z. Rao, H. Yang, Structure of M(pro) from SARS-CoV-2 and discovery of its inhibitors, *Nature* (2020), <https://doi.org/10.1038/s41586-020-2223-y>.
- [15] W.F. Kuang, L.P. Chow, M.H. Wu, L.H. Hwang, Mutational and inhibitive analysis of SARS coronavirus 3C-like protease by fluorescence resonance energy transfer-based assays, *Biochem. Biophys. Res. Commun.* 331 (2005) 1554–1559, <https://doi.org/10.1016/j.bbrc.2005.04.072>.
- [16] H. Chiang, J.C. Lee, H.C. Huang, H. Huang, H.K. Liu, C. Huang, Delayed intervention with a novel SGLT2 inhibitor NGI001 suppresses diet-induced metabolic dysfunction and non-alcoholic fatty liver disease in mice, *Br. J. Pharmacol.* 177 (2020) 239–253, <https://doi.org/10.1111/bph.14859>.
- [17] S. Jo, S. Kim, D.H. Shin, M.S. Kim, Inhibition of SARS-CoV 3CL protease by flavonoids, *J Enzyme Inhib Med Chem* 35 (2020) 145–151, <https://doi.org/10.1080/14756366.2019.1690480>.
- [18] J.M. Yang, C.C. Chen, GEMDOCK: a generic evolutionary method for molecular docking, *Proteins* 55 (2004) 288–304, <https://doi.org/10.1002/prot.20035>.
- [19] D.S. Wishart, Y.D. Feunang, A.C. Guo, E.J. Lo, A. Marcu, J.R. Grant, T. Sajed, D. Johnson, C. Li, Z. Sayeeda, N. Assempour, I. Iynkkaran, Y. Liu, A. Maciejewski, N. Gale, A. Wilson, L. Chin, R. Cummings, D. Le, A. Pon, C. Knox, M. Wilson, DrugBank 5.0: a major update to the DrugBank database for 2018, *Nucleic*

- Acids Res. 46 (2018) D1074–D1082, <https://doi.org/10.1093/nar/gkx1037>.
- [20] P. Kumberger, F. Frey, U.S. Schwarz, F. Graw, Multiscale modeling of virus replication and spread, *FEBS Lett.* 590 (2016) 1972–1986, <https://doi.org/10.1002/1873-3468.12095>.
- [21] L. Zou, F. Ruan, M. Huang, L. Liang, H. Huang, Z. Hong, J. Yu, M. Kang, Y. Song, J. Xia, Q. Guo, T. Song, J. He, H.L. Yen, M. Peiris, J. Wu, SARS-CoV-2 viral load in upper respiratory specimens of infected patients, *N. Engl. J. Med.* 382 (2020) 1177–1179, <https://doi.org/10.1056/NEJMc2001737>.
- [22] M. Jang, Y.I. Park, Y.E. Cha, R. Park, S. Namkoong, J.I. Lee, J. Park, Tea polyphenols EGCG and theaflavin inhibit the activity of SARS-CoV-2 3CL-protease in vitro, *Evid Based Complement Alternat Med* 2020 (2020) 5630838, <https://doi.org/10.1155/2020/5630838>.
- [23] L. Yi, Z. Li, K. Yuan, X. Qu, J. Chen, G. Wang, H. Zhang, H. Luo, L. Zhu, P. Jiang, L. Chen, Y. Shen, M. Luo, G. Zuo, J. Hu, D. Duan, Y. Nie, X. Shi, W. Wang, Y. Han, T. Li, Y. Liu, M. Ding, H. Deng, X. Xu, Small molecules blocking the entry of severe acute respiratory syndrome coronavirus into host cells, *J. Virol.* 78 (2004) 11334–11339, <https://doi.org/10.1128/JVI.78.20.11334-11339.2004>.
- [24] Q. Ruan, K. Yang, W. Wang, L. Jiang, J. Song, Clinical predictors of mortality due to COVID-19 based on an analysis of data of 150 patients from Wuhan, China, *Intensive Care Med.* 46 (2020) 846–848, <https://doi.org/10.1007/s00134-020-05991-x>.
- [25] P. Mehta, D.F. McAuley, M. Brown, E. Sanchez, R.S. Tattersall, J.J. Manson, U.K. Hlh, Across Speciality Collaboration, COVID-19: consider cytokine storm syndromes and immunosuppression, *Lancet* 395 (2020) 1033–1034, [https://doi.org/10.1016/S0140-6736\(20\)30628-0](https://doi.org/10.1016/S0140-6736(20)30628-0).
- [26] B.N. Singh, S. Shankar, R.K. Srivastava, Green tea catechin, epigallocatechin-3-gallate (EGCG): mechanisms, perspectives and clinical applications, *Biochem. Pharmacol.* 82 (2011) 1807–1821, <https://doi.org/10.1016/j.bcp.2011.07.093>.
- [27] J. Zhang, L. Li, S.H. Kim, A.E. Hagerman, J. Lu, Anti-cancer, anti-diabetic and other pharmacologic and biological activities of penta-galloyl-glucose, *Pharm. Res. (N. Y.)* 26 (2009) 2066–2080, <https://doi.org/10.1007/s11095-009-9932-0>.